CAO, J., WANG, S. and FERNANDEZ, C. 2024. Multi-kernel support vector regression optimization model and indirect health factor extraction strategy for the accurate lithium-ion battery remaining useful life prediction. *Journal of solid state electrochemistry* [online], 28(1), pages 19-32. Available from: https://doi.org/10.1007/s10008-023-05650-3

Multi-kernel support vector regression optimization model and indirect health factor extraction strategy for the accurate lithium-ion battery remaining useful life prediction.

CAO, J., WANG, S. and FERNANDEZ, C.

2024

Multi-kernel Support Vector Regression Optimization Model and Indirect Health Factor Extraction Strategy for the Accurate Lithium-ion Battery Remaining Useful Life Prediction

Journal:	*Journal of The Electrochemical Society*
Manuscript ID	JES-109858
Manuscript Type:	Research Paper
Date Submitted by the Author:	08-Mar-2023

Complete List of Authors:	Cao, Jie; Southwest University of Science and Technology, Wang, Shunli; Southwest University of Science and Technology Xie, Yanxin; Southwest University of Science and Technology Fernandez, Carlos; Robert Gordon University

Keywords:	Lithium-ion battery, health factor, gray wolf cuckoo search model, multi-kernel support vector regression

Multi-kernel Support Vector Regression Optimization Model and Indirect Health Factor Extraction Strategy for the Accurate Lithium-ion Battery Remaining Useful Life Prediction

Jie Cao[a], Shunli Wang[ab*], Yanxin Xie[a], Carlos Fernandez[c]

[a]*School of Information Engineering, Southwest University of Science and Technology, Mianyang 621010, China;*

[b]*College of Electrical Engineering, Sichuan University, Chengdu 610065, China;*

[c]*School of Pharmacy and Life Sciences, Robert Gordon University, Aberdeen, UK*

Abstract: Remaining Useful Life (RUL) of Lithium-ion batteries is an important indicator for battery health management, and accurate prediction can promote reliable battery system design, as well as safety and effectiveness of practical use. Therefore, we extract the health factor during charging and an improved multi-kernel support vector regression (MKSVR) RUL prediction model to achieve high accuracy estimation of the RUL of Lithium-ion batteries. Firstly, based on the current, voltage, and temperature data during charging, seven characteristic parameters that can reflect the battery capacity decay are extracted, and then, three health factors (HF) that are highly correlated with the capacity decay are screened out using Pearson coefficients. Secondly, the improved Gray Wolf Cuckoo Search Optimization (GWOCS) model is used to realize the intelligent optimization search of the kernel function parameter combinations of the multi-kernel support vector regression, and then the improved RUL prediction model of the multi-kernel support vector regression is established. Finally, the validation analysis is performed based on the NASA battery aging dataset. The results show that the improved multi-kernel support vector regression has higher prediction accuracy compared with the single-kernel support vector regression, and its RUL prediction errors are all less than 5 cycles, and the maximum root mean square error is all less than 0.028.

Keywords: Lithium-ion battery, health factor, gray wolf cuckoo search model, multi-kernel support vector regression

*Corresponding author: Shunli Wang. Tel: +86-15884655563. E-mail address: 497420789@qq.com.

1. Introduction

With the advantages of high energy density and high output power, lithium-ion batteries have an important position in the field of renewable energy[1]. As the application of lithium-ion batteries in the new energy vehicle industry becomes more and more widespread, their health status is getting more and more attention[2]. The wide application of lithium-ion batteries also brings corresponding safety problems. As the number of charge and discharge cycles of the battery increases, a series of aging reactions will occur inside it, such as capacity reduction and impedance increase[3, 4]. When the lithium-ion battery reaches the failure threshold without the corresponding safety management measures, it may lead to serious safety accidents[5, 6]. Scientific lithium battery control strategy, accurate lithium battery health state (State of health, SOH), and remaining life detection play a vital role in the full play of lithium battery performance and safety control[7].

The current prediction methods for lithium-ion battery RUL can be mainly divided into mechanism-based model prediction methods and data-driven prediction methods[8, 9]. The model approach builds the RUL prediction model by analyzing the internal mechanical structure of lithium-ion batteries[10]. Miao et al.[11] used an exponential growth type model to fit the capacity degradation curve of the battery to construct a lithium-ion battery degradation model and used a trace-free particle filtering algorithm for RUL prediction with a prediction error of less than 5%. Tian et al.[12] proposed an aging pattern identification method based on open-circuit voltage matching analysis, and established a mapping model of battery health status, ohmic resistance, and polarization resistance evolution. The results show that the model can achieve high accuracy RUL prediction and the prediction results can be maintained within the 95% confidence interval. To address the capacity regeneration phenomenon of Li-ion batteries and improve the accuracy of RUL prediction, Ma et al.[13] detected capacity regeneration points by particle filter with the Whitney U test method to update the degradation model parameters. The validation by the NASA battery dataset shows that the maximum RUL estimation error is 7 cycles and the detection rate reaches 83.3% for capacity regeneration data points. In the state estimation of particle filtering, the degradation and lack of diversity of particles can make the prediction results unreliable and inaccurate. Yang et al.[14] proposed a fused RUL prediction method with optimal combination strategy and traceless particle filter to track the degradation process of a cell with highly nonlinear characteristics and accurately predict its RUL, and OCS was used in the resampling process to improve the distribution of particle filtering and maintain diversity. The results show that the proposed method has good superiority and robustness, and the RUL prediction accuracy can be maintained above 95%. The RUL prediction method based on the machine model can improve the prediction accuracy better under relatively stable external conditions, but the accuracy of the model is easily affected by the variable current and temperature, and it is difficult to obtain an accurate mechanism model under the influence of different external conditions[15].

Data-driven methods aim to map the relationship between the input data and output data of the above mechanistic models through some approximate models built adaptively based on available data[16], such as statistical models, Neural Networks (NN)[17], Gaussian process regression[18, 19], support vector regression[20], fuzzy inference, etc. These data-driven approximate models can be broadly classified into statistical, stochastic and intelligent techniques according to the techniques used[21]. Li et al.[22] proposed a data-driven RUL prediction technique based on smoothing the capacity increment curves using a filtering algorithm and extracting the battery health features from the capacity increment curves as a training data set. Based on training datasets of different sizes, three SVR-based battery degradation models were developed. The experimental results show that the average absolute error and root mean square error of the three models are lower than 2%, in addition. The accuracy of the three models is improved by 30% in both MAE and RMSE. Xue et al.[23] proposed an integrated algorithm combining adaptive traceless Kalman filtering and genetic algorithm to optimize support vector regression (GA-SVR). The AUKF algorithm was used to adaptively update process noise and observation noise, and then the GA algorithm was used to optimize the parameter selection process of SVR to achieve multi-step prediction of RUL. The results show that the proposed AUKF-GA-SVR algorithm has high RUL prediction accuracy and the prediction error can be controlled within 6 cycles. Wang et al.[24] proposed a transferable method for predicting the lifetime of lithium-ion batteries to solve the current error accumulation problem and the inapplicability of the remaining battery life model under different operating conditions. The battery degradation data is mapped into a subspace by building an encoding net that can extract the global battery degradation information. And a novel RUL prediction method is constructed by using a cyclic consistency learning method to train the coding net. The experimental results show that the method can achieve high prediction accuracy and also provide a new direction for RUL prediction.

Although all these papers achieved good prediction results on RUL prediction, they all used single kernel SVR models or RVM models, which failed to fully exploit the advantages of these models. Some scholars have started to study regression models with multi-kernel functions. Lyu et al.[25] proposed an indirect hybrid model for online battery prediction and health management (PHM) using GWO to optimize a multi-kernel correlation vector machine (MKRVM) to determine the weights and kernel parameters of different kernel functions. The results show that the indirect hybrid model has high flexibility and strong robustness for battery PHM. The above studies have achieved accurate prediction of RUL by different aspects, but these studies still have some shortcomings in some aspects, so this study tries to establish a more effective method for extracting the health factor of lithium-ion batteries.

To synthesize the above, to more accurately characterize the dynamic properties and aging phenomena of batteries, this study investigates and analyzes three aspects of health factors, multi-kernel support vector regression and GWOCS intelligent search algorithm to achieve high accuracy estimation of RUL of Lithium-ion batteries.

2. Theoretical Analysis

2.1 Lithium-ion battery health factor extraction

The lithium-ion battery aging dataset used in this study is from NASA PCoE Research Center, and this dataset contains experimental data on charge/discharge cycles of several rechargeable lithium-ion batteries. In this study, B0005 and B0006 batteries with a rated capacity of 2Ah and a cutoff voltage of 4.2V during charging were selected as the experimental subjects.

The decay of capacity and the change of internal resistance data of lithium-ion batteries in practical applications are difficult to obtain directly, and it is difficult to extract stable indirect HF from the discharge data because of the interference received from various usage habits and external factors during the battery discharge process[26]. In contrast, the battery charging process is relatively stable, and it is easier to extract indirect health factors with characteristic representativeness to better predict the RUL of Lithium-ion batteries[27]. therefore, this study extracts seven sets of indirect HF data related to current, voltage and temperature based on the data sets of batteries B5 and B6, after analyzing numerous curve variation patterns. Taking the B5 battery as an example, the extracted health factors are as follows.

1. For the same battery, the difference in current drop (Current Difference, CD) exists after the same charging time Δt due to the different rates of the current drop in different cycles, as shown in Fig.1 (a). The formula for calculating CD is shown in Eq. (1).

$$CD(\Delta I) = 1.5 - I_t \tag{1}$$

2. As shown in Fig.1 (b), the rate of charge voltage rise is different for different cycles in the same battery data set. Similarly, the voltage difference (VD) between the same charging time Δt and the rated voltage 4.2 V is also different. the formula for calculating VD is shown in Eq. (2).

$$VD(\Delta V) = 4.2 - V_t \tag{2}$$

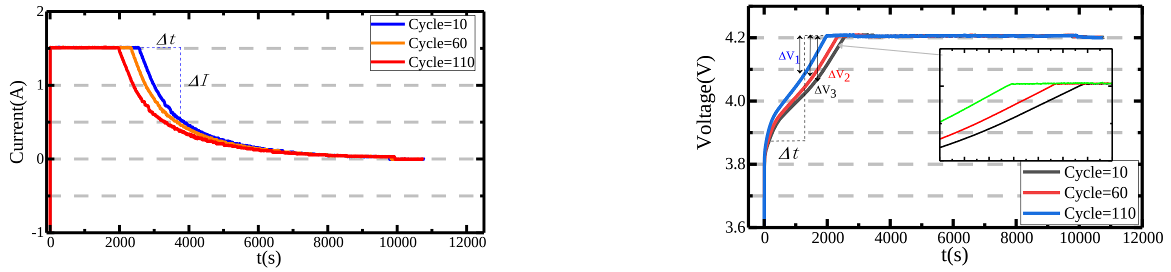

(a) Charging current at different cycle times (b) Charging voltage at different cycle times

Fig. 1 Current-voltage curve of B5 battery at different cycle times

3. As shown in Fig.2, the maximum temperature reached by the battery during charging is different in different cycles and the time to reach the maximum temperature is also different, so it is reasonable to use the time to reach the maximum temperature (Max temperature Time, MT) to reflect the battery aging phenomenon.

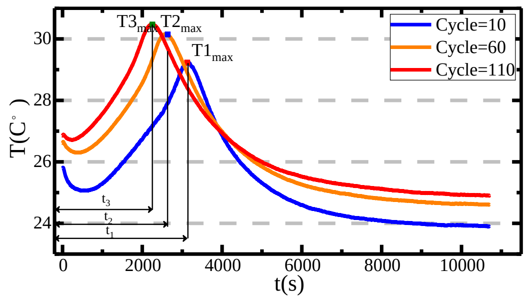

Fig. 2 Temperature change during charging

The HF extracted at this time includes a total of 6 groups of CD and VD of Δt = 500, 1000, 1500, and a set of MT. where the extracted CD and VD scatter plots are shown in Fig. 3.

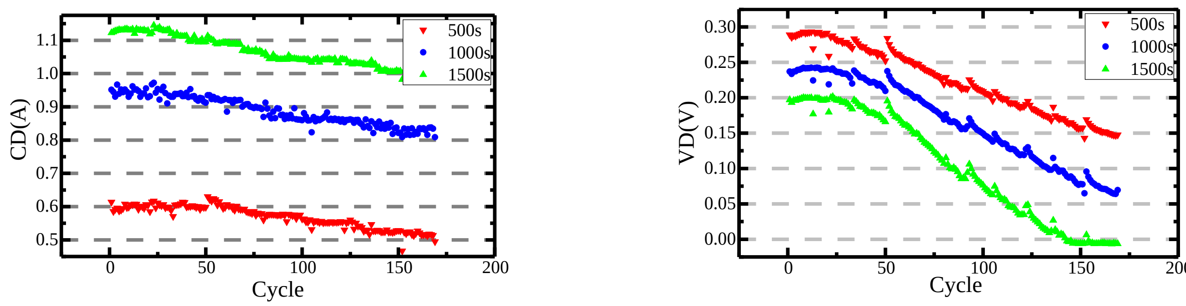

(a) CD at different time intervals (b) VD at different time intervals

Fig. 3 Trends in CD and VD at different time intervals

As can be seen from Fig.3, as the number of cycles of the Lithium-ion battery increases, the available capacity of the battery decreases and both CD and VD show a decreasing trend. Fig.4 shows the time required for the battery to reach the maximum temperature during the charging process.

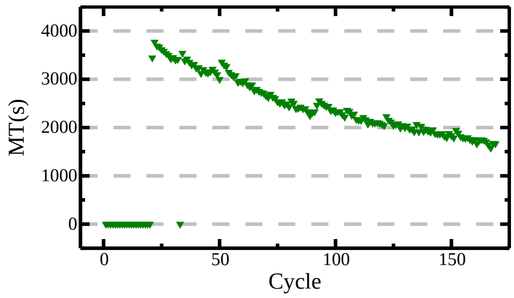

Fig. 4 Time required to reach maximum temperature

Due to the battery data set, the charging data of the initial 25 cycles did not contain the maximum temperature value, so the initial 25 MT values were all 0. It can be seen from Fig. 4 that the trend of MT is in high agreement with the trend of battery capacity decay. The above results tentatively indicate that it is feasible to use HF to indirectly characterize the capacity decay process of Lithium-ion batteries.

2.2 Health factor correlation analysis

To investigate the correlation between the lithium-ion battery capacity decay and the HF extracted above, the data with a higher correlation is further screened to reduce the cost of model training. Pearson correlation coefficient is used for correlation analysis. The formula of the Pearson coefficient is shown in Eq. (3).

$$P_{XY} = \frac{\operatorname{cov}(X,Y)}{\sigma_X \sigma_Y} = \frac{E(XY) - E(X)E(Y)}{\sqrt{E(X^2) - E^2(X)}\sqrt{E(Y^2) - E^2(X)}} \tag{3}$$

In Eq. (3), X denotes the extracted HF data and Y denotes the lithium-ion battery capacity decay data. $cov(X,Y)$ denotes the covariance of X, Y. σ_X and σ_Y denotes the standard deviation. From the principle of the Pearson coefficient, it is known that when the Pearson coefficient is greater than 0.9, it is proved that the HF is extremely correlated with the battery capacity decay. Tab.1 shows the Pearson coefficients obtained by calculating the seven sets of HF data extracted from the B5 battery data set with the battery capacity.

Tab. 1 Pearson correlation coefficient

Battery	Health factors	Pearson coefficient
B5	CD (500s)	0.8823
	CD (1000s)	0.9184

	CD (1500s)	0.9579
	VD (500s)	0.8763
	VD (1000s)	0.8940
	VD (1500s)	0.9466
	MT	0.9578

From Tab.1, we can see that all seven HF data sets have a high correlation with the battery capacity, which proves that the previous method of selecting HF has high feasibility. To ensure that the extracted HF can have stronger generalization, we select HF data sets with Pearson correlation coefficients above 0.94 as the input of the model. Therefore, the three data sets CD (1500S), VD (1500S) and MT will be used as the input training data sets for the GWOCS-MKSVR model.

2.3 Analysis of the Gray Wolf Optimization Search Algorithm

Gray Wolf Optimizer (GWO) algorithm is better for complex constraints and searching unknown spaces commonly found in practical engineering[28], but it is easy to fall into local optimum when facing high dimensional problems[29]. The Cuckoo Search (CS) algorithm is an optimization algorithm proposed in combination with Lévy Flights[30], which has a better global search performance. The above 2 algorithms are combined to form the GWOCS algorithm, which perturbatively updates the population position during the iteration process, which can effectively increase the population diversity and balance the global and local search ability of the algorithm.

The gray wolves in a wolf pack follow a pyramidal social dominance hierarchical relationship, and their hierarchical distribution is shown in Fig.5. According to this relationship, the gray wolf pack can be divided into four classes: α wolves, β wolves, δ wolves and ω wolves[31]. In the wolf pack, the lower wolves need to obey the higher wolves, and the pack balances the internal relationship accordingly. GWO algorithm uses the hierarchical relationship of the wolf pack, constructs a model, calculates the fitness of each wolf, and ranks the wolves according to the size of the fitness, and selects the top 3 wolves in the fitness as α wolves, β wolves, δ wolves, and the rest as ω wolves. GWO optimization can be described as the process of prey tracking and siege by ω wolves following α, β, and δ wolves, the location of the prey is the optimal solution[32].

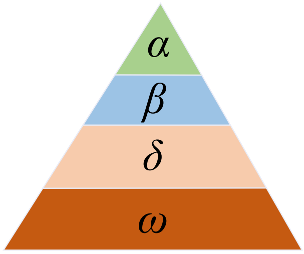

Fig. 5 Gray Wolf Hierarchy Mechanism

The specific steps of the GWO algorithm are as follows:

Step 1: Search for Prey.

$$D = |CX_p(t) - X(t)| \tag{4}$$

$$X(t+1) = X_p(t) - AD \tag{5}$$

In Eq. (4), D is the distance of the prey, $X_p(t)$ is the position of the prey in the t th generation, $X(t)$ is the position of the gray wolf in the t th generation, $C = 2r_i$ denotes the coefficient vector, which controls the wolf pack activity, and r_i is a random number within 0 to 1. In Eq. (5), $X(t+1)$ denotes the updated position of the $t+1$th generation of gray wolves; A is the convergence vector, which controls the wolves' actions[33].

$$A = 2ar_i - a \tag{6}$$

In Eq. (6), the initial value of a is 2, which decreases linearly with the number of iterations until it decreases to 0.

Step: Surrounding the prey.

At the beginning of the hunt, it is assumed that α wolf position is optimal, and the prey is pursued by leading β and δ. The distances of α, β, and δ from the prey are determined according to Eq. (7).

$$D_k = |C_i X_k(t) - X(t)| \tag{7}$$

$$\begin{cases} X_1 = X_\alpha - A_1 D_\alpha \\ X_2 = X_\beta - A_2 D_\beta \\ X_3 = X_\delta - A_3 D_\delta \end{cases} \tag{8}$$

In Eq. (7), k denotes α, β, δ, i = 1, 2, 3. In Eq. (8), X_1, X_2, X_3 denotes the distance and direction of ω wolves advancing toward α, β, δ wolves. A_1, A_2, A_3 denotes the coefficient vectors.

$$X(t+1) = \frac{X_{w\alpha} + X_{w\beta} + X_{w\delta}}{3} \tag{9}$$

Eq. (9) indicates that ω wolves update their positions according to the positions of α, β, and δ wolves.

Step 3: Attacking the prey.

The gray wolf pack attacks the prey when the prey stops moving, giving the algorithm a good local fine search capability. The construction of the attack model needs to be completed by decreasing the value of a[34]. In Eq. (6), because a is decreasing during the iteration, A fluctuates in the interval $-a$ to a, and when A is between -1 to 1, the next position of the gray wolf is between the current position and the prey position. When $|A|>1$, the search for the prey continues.

2.4 Analysis of the Gray Wolf-Cuckoo Search Algorithm

In the iterative process of the GWO algorithm, the wolves always update their positions according to the position information of α wolves, β wolves and δ wolves, which easily leads the wolves into the local optimal position and the global search ability is weak. In contrast, the Lévy flight mechanism in the CS algorithm is a typical random wandering way, and the algorithm searches for steps with almost equal probability of length and has high selectivity of moving direction, which can update the nest position randomly and complete the global search[35]. The Lévy flight process is shown in Eq. (10).

$$x_i^{t+1} = x_i^t + \alpha \cdot L(\lambda) \tag{10}$$

In Eq. (10), X_i^t is the position of the t th generation of the i th cuckoo; X_i^{t+1} is the position of the new generation of cuckoo; α is the step scaling factor; λ is the Lévy index; $L(\lambda)$ is the random search step satisfying the Lévy flight distribution. The calculation formula is shown in Eq. (11).

$$L(\lambda) = \frac{\mu}{|v|^{\frac{1}{\lambda}}} \tag{11}$$

In Eq. (11), μ and v represent two random numbers obeying normal distribution. According to the above equation, the CS algorithm decides that some individuals obey the random wandering of Lévy flight according to the discovery probability, and completes the population update in the way shown in Eq. (12).

$$X_g(t+1) = X_g(t) + \gamma \oplus L(\lambda) \tag{12}$$

In Eq. (12), $X_g(t+1)$ and $X_g(t)$ denote the updated position of the g th nest as well as the current position; γ denotes the random number of individual positions. Therefore, the two can be combined to build the gray wolf-cuckoo fusion search algorithm. The flow chart of the fusion algorithm is shown in Fig. 6.

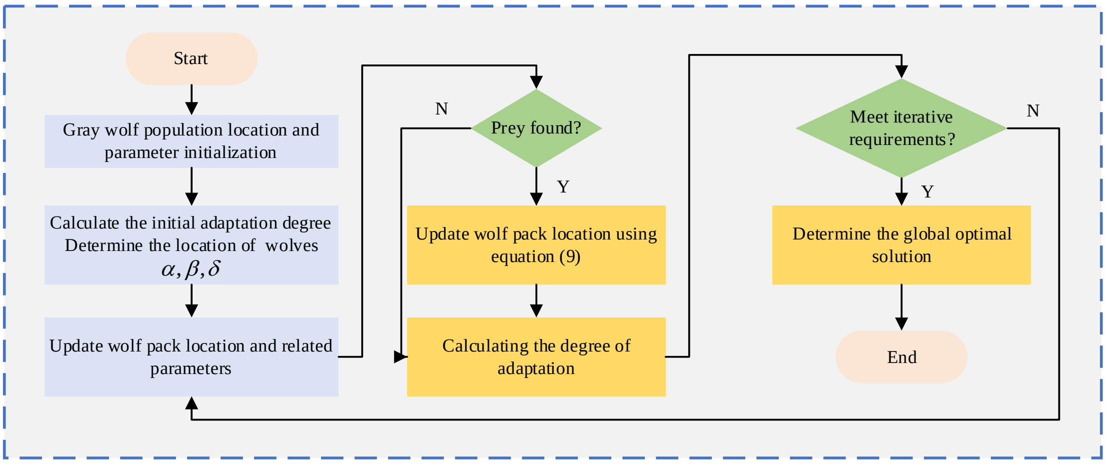

Fig. 6 Flowchart of GWOCS optimization search algorithm

In the GWOCS optimization algorithm, after the prey is found, the position update method in the CS algorithm is used to update the position of the wolf pack in the next stage to avoid the wolf pack from falling into the local optimal solution.

2.5 Multi-kernel support vector regression

A multi-kernel model offers higher flexibility than a single-kernel function. In the context of multi-kernel mapping, the high-dimensional space becomes a combinatorial space made by combining multiple feature spaces. Since the combinatorial space gives full play to the different feature mapping capabilities of each basic kernel, it can solve the different feature components of heterogeneous data by the corresponding kernel functions respectively. At present, the mainstream multi-kernel learning methods include linear kernel, multi-scale kernel and infinite kernel. The linear combinations of kernel functions are usually relatively stable and can perform the basic functions of kernel functions. Through the linear combination of multiple kernel functions, the advantages of each kernel function can be combined to improve the prediction ability of the model. The expression of the combined kernel function model constructed in this paper is shown in Eq. (13).

$$K_{combo}(x, x_i) = w_1 K_{ploy}(x, x_i) + w_2 K_{liner}(x, x_i) + w_3 K_{RBF}(x, x_i) \tag{13}$$

In Eq. (13), w_1, w_2 and w_3 denote the weight coefficients of each linear combination of kernel functions in the multi-kernel function. $w_1 + w_2 + w_3 = 1$, and $w_1, w_2, w_3 > 0$.

$K_{ploy}(x, x_i)$ denotes the polynomial kernel function, which serves to achieve global generalization. $K_{liner}(x, x_i)$ denotes the linear kernel function, which enables tracking of the global monotonic trend. $K_{RBF}(x, x_i)$ denotes the Gaussian kernel function, also called the radial basis kernel function, which achieves the capture of local nonlinear features. The expressions of these three different kernel functions are shown in Eq. (14).

$$\begin{cases} K_{ploy}(x, x_i) = (x \cdot x_i^T + 1)^d \\ K_{RBF}(x, x_i) = \exp(-\dfrac{\|x - x_i\|^2}{2\gamma^2}) \\ K_{liner}(x, x_i) = x \cdot x_i^T \end{cases} \tag{14}$$

In Eq. (14), γ represents the kernel parameter of the Gaussian kernel function and d is the order of the polynomial kernel function. the detailed derivation formula of the SVR model has been derived in detail in the literature[23]. Based on this, the expression of MKSVR can be derived as shown in Eq. (15), where a_i and a_i^* are Lagrange multipliers.

$$\begin{aligned} f(x) &= \sum_{i=1}^{n}(a_i - a_i^*)K_{combo}(x, x_i) + b \\ &= \sum_{i=1}^{n}(a_i - a_i^*)(w_1 K_{ploy}(x, x_i) + w_2 K_{liner}(x, x_i) + w_3 K_{RBF}(x, x_i)) + b \end{aligned} \tag{15}$$

In the NASA dataset, the overall trend of the lithium-ion battery capacity degradation curve is monotonically decreasing, so the choice of linear kernel function and Gaussian kernel function can effectively characterize the local nonlinearities in the degradation process. Secondly, it is necessary to include polynomial kernel functions to achieve global generalization because the historical data will have an impact on the current RUL estimation. In this paper, the MKSVR model is trained using the extracted 3 sets of HF as the training data input to the model, and the combined coefficients of the fusion kernel function are optimized centrally using the GWOCS optimization-seeking algorithm. The flow chart of the GWOCS-based multi-kernel SVR fusion model is shown in Fig.7.

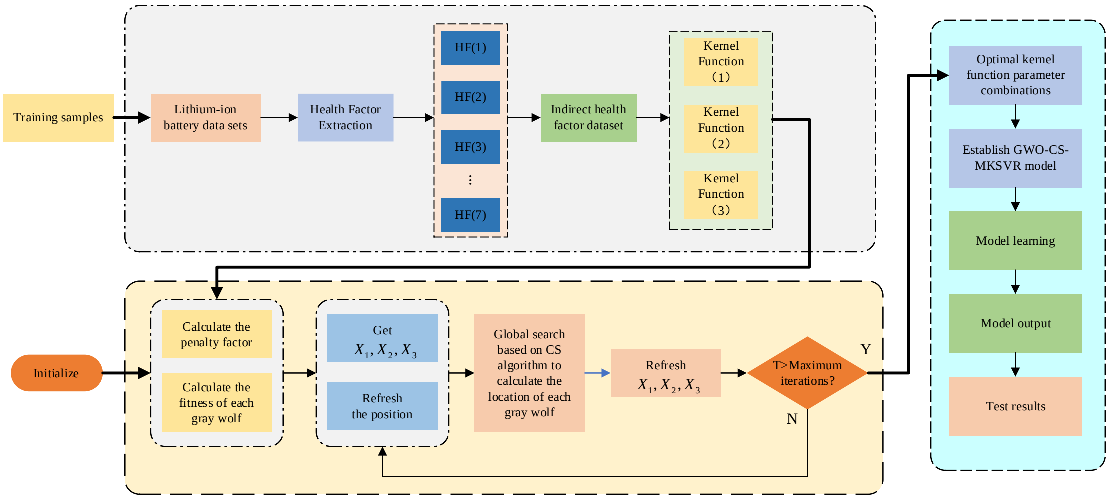

Fig. 7 The flowchart of the multi-kernel SVR fusion model based on GWOCS optimization

The steps of RUL prediction based on GWOCS with multi-kernel SVR are as follows:

1. Data pre-processing. To achieve higher accuracy in RUL prediction, health factors need to be extracted from the aging data. After completing the correlation analysis, the health factor data set with a higher correlation is selected as the model training input.
2. Multi-kernel SVR kernel function parameters are optimized. MKSVR takes Eq. (15) as the kernel function, based on which the combination of kernel function coefficients is obtained with the GWOCS optimization algorithm.
3. RUL prediction. The GWOCS-MKSVR model is constructed for training and achieves high-accuracy RUL prediction.

3. Validation analysis of experimental results

In this section, the RUL prediction analysis is performed on the aging dataset of B5 and B6 batteries from NASA PCoE Research Center based on the HF extraction mentioned in Section II and the GWOCS-MKSVR model. To evaluate the performance of the algorithm, a comparative analysis is performed using the single-kernel SVR and MKSVR with the improved model. In addition, the mean absolute error (MAE) and root mean square error (RMSE) is introduced as the evaluation index of the algorithm performance. The formulas of MAE and RMSE are shown in Eq. (16) and Eq. (17).

$$MAE = \frac{1}{N}\sum_{i=1}^{N}| x_i - \hat{x}_i | \tag{16}$$

$$RMSE = \sqrt{\frac{1}{N}(\sum_{i=1}^{N}(x_i - \hat{x}_i)^2)} \tag{17}$$

3.1 Experimental verification at start cycle=60

In the B5 and B6 battery data sets, there are 168 charge/discharge cycles of battery capacity data. We use the first 60 and first 70 cycles as the model offline training data set, and the last 108 and last 98 cycles as the model prediction data set, and the starting point of RUL prediction is start cycle (SC) = 60, 70. Since the starting capacity of the two batteries is 2Ah, the batteries are regarded as obsolete when the actual available capacity is 70% of the rated capacity, so the RUL In the prediction process, the failure threshold is set to 1.4Ah.

Fig.8 represents the RUL prediction results for the B5 and B6 battery data sets at SC=60. In Fig.8(a), C1 represents the real capacity degradation curve of the battery, C2 represents the RUL prediction results obtained by the GWOCS-MKSVR optimization model, and C3 and C4 are used as comparison curves to verify the performance of the improved model, representing the prediction results of the single-kernel SVR algorithm and the prediction results of the MKSVR algorithm, respectively.

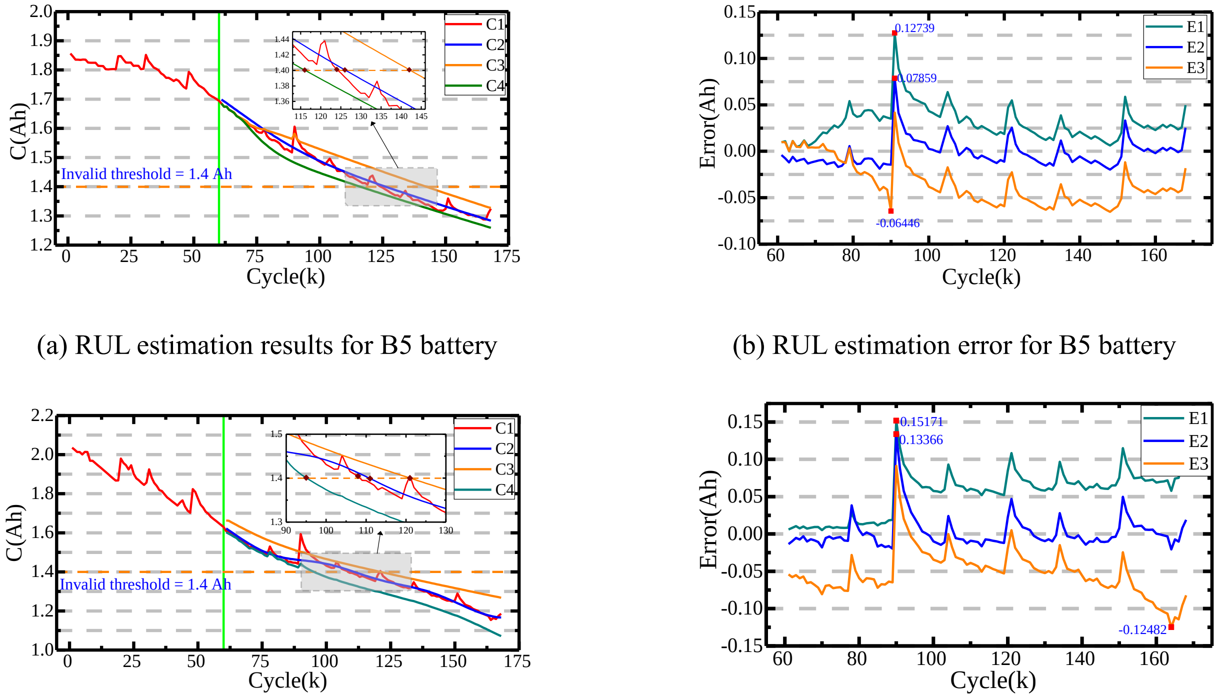

(a) RUL estimation results for B5 battery (b) RUL estimation error for B5 battery

(c) RUL estimation results for B6 battery (d) RUL estimation error for B6 battery

Fig. 8 RUL estimation results at SC=60

Fig.8(a) shows the RUL prediction results for the B5 battery. The magnified plot shows that the true failure threshold of the battery is 124, the predicted failure threshold of the improved algorithm is 126, the predicted failure threshold of the SVR algorithm is 142 and the predicted failure threshold of MKSVR is 116. the RUL prediction performance of the algorithm can be described more intuitively by Eq. (18) and Eq. (19), in which RUL_{pre} denotes the RUL prediction value and RUL_{real} denotes the true RUL value of the battery. In Eq. (19), RUL_e denotes the relative error of the predicted value.

$$Error_{pre} = \left| RUL_{pre} - RUL_{real} \right| \tag{18}$$

$$RUL_e = \frac{\left| RUL_{pre} - RUL_{real} \right|}{RUL_{real}} \times 100\% \tag{19}$$

In the RUL prediction of B5 battery, the single-kernel SVR algorithm can simulate the capacity decay trend of the battery, but its prediction error is large, and the error between the predicted value and the real value is 18 cycles. MKSVR improves the shortcomings of the single-kernel SVR to a certain extent, and its simulation prediction error is 8 cycles. The GWOCS-MKSVR model can achieve the simulation of battery capacity decay trend well, and the prediction error is only 2 cycles. Fig.8(c) shows the RUL prediction results for battery B6, where the true battery failure threshold is 108, the single-kernel SVR prediction is 121, the MKSVR prediction is 95, and the MKSVR has better tracking than the SVR. the GWOCS-MKSVR prediction is 111, and the model has the best tracking among these three models, indicating that for the GWOCS The search mechanism plays a positive role in the optimization of the parameter selection of the multi-kernel function. The specific error comparison results are shown in Tab. 2.

Tab. 2 Comparison of RUL prediction results of different algorithms at SC=60

Estimation algorithm	SVR		MKSVR		GWOCS-SVR	
Battery	B5	B6	B5	B6	B5	B6
$Error_{pre}$	18	13	8	13	2	3
RUL_e	14.516%	12.037%	6.451%	12.037%	1.612%	2.777%

As can be seen from Tab. 2, the RUL prediction accuracy of the GWOCS-MKSVR model is greatly improved compared with both the SVR and MKSVR models when predicting for the B5 cell, and the RUL estimation error period is greatly reduced, and the estimation accuracy is improved by 12.904% and 4.839%, respectively. The estimation accuracy of the GWOCS-MKSVR model is improved by 9.26% when predicting the B6 cell. In Fig. 8(b) and Fig. 8(d), E1 represents the estimation error curve of the MKSVR model, E2 represents the estimation error curve of GWOCS-MKSVR, and E3 represents the estimation error curve of SVR. It can be seen that the maximum estimation errors of E2 are 0.07859 and 0.13366, the maximum errors of E1 are 0.12739 and 0.15171, and the maximum errors of E3 are -0.06446 and -0.12482, respectively. although the error of E3 is the smallest, the tracking is poor and it is difficult to simulate the real capacity decay trend of the battery. the error curve of E2 always fluctuates around The E2 error curve fluctuates around 0, which is more stable and convergent than the traditional algorithm. The specific performance index can be calculated by Eq. (18) and Eq. (19), and the calculation results are shown in Tab.3.

Tab. 3 RUL estimation error indicator at SC=60

Battery	Algorithm	MAE	RMSE
B0005	SVR	0.0365	0.0414
	MKSVR	0.0203	0.0256
	GWOCS-MKSVR	0.0107	0.0145
B0006	SVR	0.0550	0.0604
	MKSVR	0.0324	0.0452
	GWOCS-MKSVR	0.0133	0.0216

As can be seen in Tab. 3, compared with SVR and MKSVR, GWOCS-MKSVR prediction error metrics are smaller and have better prediction performance, whether using B5 battery data or B6 battery data. Based on the B5 battery data set, for the MAE and RMSE of capacity prediction error, GWOCS-MKSVR is reduced respectively. Based on the data in Tab. 3, a more intuitive performance comparison graph can be obtained, as shown in Fig. 9.

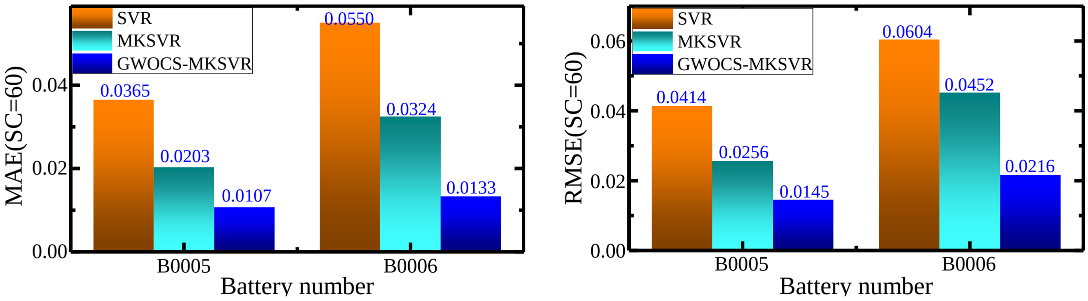

(a) MAE Comparative Analysis (b) RMSE Comparative Analysis

Fig. 9 Comparison of MAE and RMSE of estimation results at SC=60

From Fig. 9(a), the MAEs of the GWOCS-MKSVR model for the RUL prediction results of the B5 and B6 cell data sets are 0.0107 and 0.0133 at SC=60. compared with the SVR model, the RMSEs are reduced by 0.0258 and 0.0417, respectively. compared with the MKSVR model, the RMSEs are reduced by 0.0096 and 0.0191, respectively. In Fig. 9(b), the RMSEs of the GWOCS-MKSVR model are only 0.0145 and 0.0216, which are reduced by 0.0269 and 0.0388, respectively, compared with the SVR model, and 0.0111 and 0.0236, respectively, compared with the MKSVR model. the comparative analysis of MAE and RMSE performance indexes shows that GWOCS-MKSVR model has good prediction ability and stronger convergence, which proves that the algorithm has high reliability of prediction results and is more advantageous than the single-kernel SVR model.

3.2 Experimental verification at start cycle=70

Fig.10 shows the RUL prediction results for the B5 and B6 data sets when SC=70. In the RUL prediction results plot, C1 represents the real battery capacity degradation curve, C2 represents the RUL prediction results of the GWOCS-MKSVR model, and C3 and C4 represent the prediction results of SVR and MKSVR, respectively.

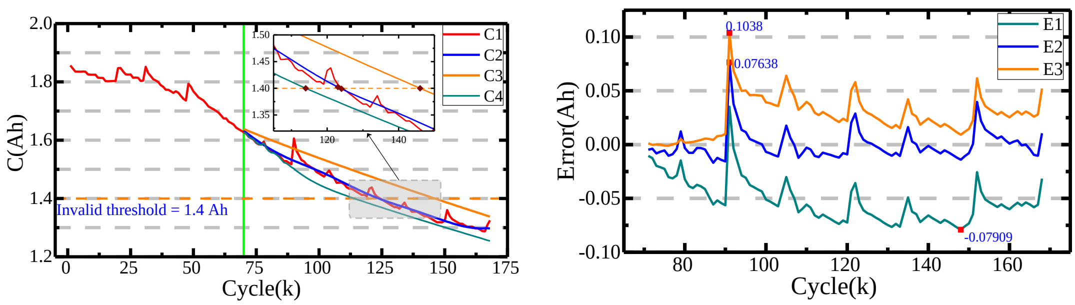

(a) RUL estimation results for B5 battery (b) RUL estimation error for B5 battery

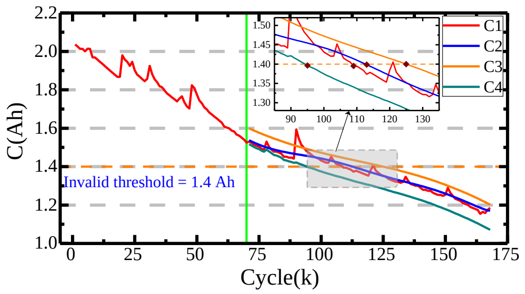

(c) RUL estimation results for B6 battery

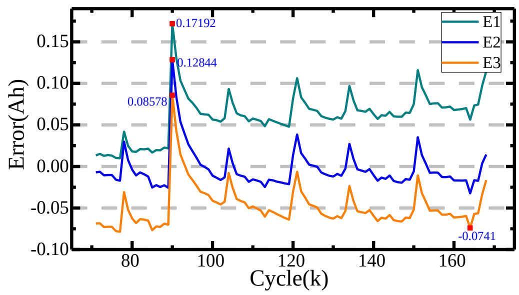

(d) RUL estimation error for B6 battery

Fig. 10 RUL estimation results at SC=70

Fig.10(a) shows the RUL prediction results for the B5 battery. As can be seen from the enlarged figure, the real RUL count of the battery is 124 cycles with 1.4Ah as the battery failure threshold, and the RUL predicted by the GWOCS-MKSVR model is 123 cycles. In contrast, the predictions of SVR and MKSVR are worse. the predicted RUL count of SVR is 146, which differs from the true value by 22, and the predicted RUL count of MKSVR is 114, with an error of 10 cycles. Fig.10(c) shows the RUL prediction results for the B6 battery. The true number of cycles available for the battery is 108, while the GWOCS-MKSVR model predicts 113. 125 for SVR and 95 for MKSVR. a more intuitive comparison of the results is shown in Tab. 4.

Tab. 4 Comparison of RUL prediction results of different algorithms at SC=70

Estimation algorithm	SVR		MKSVR		GWOCS-SVR	
Battery	B5	B6	B5	B6	B5	B6
$Error_{pre}$	22	17	10	13	1	5
RUL_e	17.741%	15.740%	8.064%	12.037%	0.806%	4.629%

As can be seen from Tab. 4, although the SVR model can achieve the prediction of battery RUL, the number of errors is large and it is difficult to achieve accurate prediction. although MKSVR has improved based on the SVR model and the prediction accuracy has been improved, the prediction error is still large, and the minimum prediction error has 10 cycles. And GWOCS-MKSVR model overcomes the shortcomings of SVR and MKSVR generalization ability and global search ability. Using the prediction accuracy of SVR and MKSVR as a comparison, the prediction accuracy of the improved model was improved by 16.935% and 7.258%, respectively, when predicting the B5 battery. When the prediction is performed for B6 cells, the improved algorithm prediction accuracy is improved by 11.111% and 7.408%, respectively. The effectiveness of the GWOCS-MKSVR model is demonstrated with higher accuracy in predicting RUL. The error analysis of Fig.10(b) and Fig.10(d) can be more visually represented by Fig. 11.

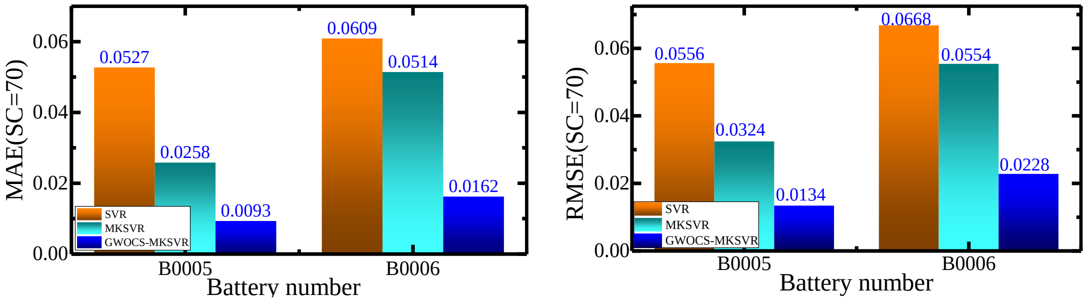

(a) MAE Comparative Analysis (b) RMSE Comparative Analysis

Fig. 11 Comparison of MAE and RMSE of estimation results at SC=70

As can be seen in Fig. 11(a), the MAE of the GWOCS-MKSVR model for the RUL prediction results for the B5 and B6 datasets is 0.0093 and 0.0162, respectively, when SC=70. compared to the SVR model, it is reduced by 0.0434 and 0.0447, respectively. compared to the MKSVR model, it is reduced by 0.0165 and 0.0352, respectively. while in Fig. 11(b), the RMSEs of the GWOCS-MKSVR model are only 0.0134 and 0.0228, which are both reduced to a larger extent compared with the SVR model and the MKSVR model, proving that increasing the number of training data can improve the accuracy of the prediction results to some extent, and further proving that the improvement of the GWOCS-MKSVR model is effective in terms of accuracy and convergence.

According to the above comparative analysis, the GWOCS-MKSVR model has stronger adaptability and generalization ability than the SVR model and the MKSVR model through the mixture of multiple kernel functions and the use of the GWOCS optimization algorithm to optimize the kernel function parameters, which can achieve better tracking results for strongly nonlinear data and further improve the accuracy of RUL prediction. The model is also able to achieve good prediction results with different sets of training data, further demonstrating the strong adaptability of the model.

4. Conclusion

The safe and efficient use of Lithium-ion batteries relies heavily on the accurate prediction of RUL. To achieve more accurate RUL prediction results, this paper provides an in-depth analysis of the current status of RUL research in recent years and proposes a GWOCS-MKSVR-based RUL prediction model, which improves the single-kernel SVR model into a multi-kernel SVR model, thus increasing the adaptability and generalization of the SVR model. The GWOCS optimization-seeking algorithm is also proposed to solve the problem that the GWO algorithm easily falls into the local optimal solution by using the Levy flight mechanism in the CS algorithm, and achieves the optimal parameter combination selection of the multi- kernel function, which overcomes the problem of insufficient generalization ability in the multi-kernel SVR due to the fixed parameters of the kernel function. The problems of fewer input features for RUL prediction and poor nonlinear tracking ability and inaccurate prediction of single-kernel SVR models are solved. Finally, the prediction ability of the improved model is verified using the NASA battery aging experimental data set. Based on the experimental results as well as the analysis, it can be seen that the GWOCS-MKSVR model can achieve high accuracy RUL prediction, and the prediction accuracy can be achieved above 95.4% in all cases. The model also has smaller MAE and RMSE, better prediction stability and adaptability, and stronger prediction ability for strongly nonlinear data. This study provides a solid theoretical basis for the accurate prediction of RUL of lithium-ion batteries, which has a positive significance for the safe and efficient use of batteries.

Although the proposed GWOCS-MKSVR model can achieve high accuracy in RUL prediction, it is difficult to accurately characterize the capacity mutation caused by the capacity regeneration phenomenon during the battery aging process. This part will be investigated in depth in subsequent studies.

Acknowledgments

The work was supported by the National Natural Science Foundation of China (No. 61801407).

Data Availability Statement

The data that support the findings of this study are available from the corresponding author upon reasonable request.

References

[1] ZHAO S, GUO Z, YAN K, et al. *Towards High-energy-density Lithium-ion Batteries: Strategies for Developing High-capacity Lithium-rich Cathode Materials* [J]. 2020.

[2] ZHANG H, LIU X, LI H H, et al. *Challenges and Strategies for High-Energy Aqueous Electrolyte Rechargeable Batteries* [J]. Angewandte Chemie-International Edition, 2021, 60(2) : 598-616.

[3] MOOSAVI A, LJUNG A L, LUNDSTROM T S. *Design considerations to prevent thermal hazards in cylindrical lithium-ion batteries: An analytical study* [J]. Journal of Energy Storage, 2021, 38.

[4] HE B, LIU L, ZHANG D. *Digital Twin-Driven Remaining Useful Life Prediction for Gear Performance Degradation: A Review* [J]. Journal of Computing and Information Science in Engineering, 2021, 21(3).

[5] HASIB S A, ISLAM S, CHAKRABORTTY R K, et al. *A Comprehensive Review of Available Battery Datasets, RUL Prediction Approaches, and Advanced Battery Management* [J]. Ieee Access, 2021, 9: 86166-93.

[6] WANG Y J, TIAN J Q, SUN Z D, et al. *A comprehensive review of battery modeling and state estimation approaches for advanced battery management systems* [J]. Renewable & Sustainable Energy Reviews, 2020, 131.

[7] WANG F K, AMOGNE Z E, TSENG C, et al. *A hybrid method for online cycle life prediction of lithium-ion batteries* [J]. International Journal of Energy Research, 2022, 46(7) : 9080-96.

[8] ZHANG H, MO Z L, WANG J Y, et al. *Nonlinear-Drifted Fractional Brownian Motion With Multiple Hidden State Variables for Remaining Useful Life Prediction of Lithium-Ion Batteries* [J]. Ieee Transactions on Reliability, 2020, 69(2) : 768-80.

[9] TAN X J, TAN Y Q, ZHAN D, et al. *Real-Time State-of-Health Estimation of Lithium-Ion Batteries Based on the Equivalent Internal Resistance* [J]. Ieee Access, 2020, 8: 56811-22.

[10] YANG X, WANG S L, XU W H, et al. *Fuzzy adaptive singular value decomposition cubature Kalman filtering*

algorithm for lithium-ion battery state-of-charge estimation [J]. International Journal of Circuit Theory and Applications, 2022, 50(2) : 614-32.

[11] MIAO Q, XIE L, CUI H J, et al. *Remaining useful life prediction of lithium-ion battery with unscented particle filter technique* [J]. Microelectronics Reliability, 2013, 53(6) : 805-10.

[12] TIAN J Q, XU R L, WANG Y J, et al. *Capacity attenuation mechanism modeling and health assessment of lithium-ion batteries* [J]. Energy, 2021, 221.

[13] MA Q H, ZHENG Y, YANG W D, et al. *Remaining useful life prediction of lithium battery based on capacity regeneration point detection* [J]. Energy, 2021, 234.

[14] YANG J S, FANG W G, CHEN J Y, et al. *A lithium-ion battery remaining useful life prediction method based on unscented particle filter and optimal combination strategy* [J]. Journal of Energy Storage, 2022, 55.

[15] ZHANG Q C, LI X, ZHOU C, et al. *State-of-health estimation of batteries in an energy storage system based on the actual operating parameters* [J]. Journal of Power Sources, 2021, 506.

[16] VENUGOPAL P, SHANKAR S S, JEBAKUMAR C P, et al. *Analysis of Optimal Machine Learning Approach for Battery Life Estimation of Li-Ion Cell* [J]. Ieee Access, 2021, 9: 159616-26.

[17] CHEN L, DING Y H, LIU B H, et al. *Remaining useful life prediction of lithium-ion battery using a novel particle filter framework with grey neural network* [J]. Energy, 2022, 244.

[18] DENG Z W, HU X S, LI P H, et al. *Data-Driven Battery State of Health Estimation Based on Random Partial Charging Data* [J]. Ieee Transactions on Power Electronics, 2022, 37(5) : 5021-31.

[19] JIA J F, LIANG J Y, SHI Y H, et al. *SOH and RUL Prediction of Lithium-Ion Batteries Based on Gaussian Process Regression with Indirect Health Indicators* [J]. Energies, 2020, 13(2).

[20] LI X, MA Y, ZHU J J. *An online dual filters RUL prediction method of lithium-ion battery based on unscented particle filter and least squares support vector machine* [J]. Measurement, 2021, 184.

[21] KONG D P, WANG S H, PING P. *State-of-health estimation and remaining useful life for lithium-ion battery based on deep learning with Bayesian hyperparameter optimization* [J]. International Journal of Energy Research, 2022, 46(5) : 6081-98.

[22] LI X Y, YUAN C G, WANG Z P. *State of health estimation for Li-ion battery via partial incremental capacity analysis based on support vector regression* [J]. Energy, 2020, 203.

[23] XUE Z W, ZHANG Y, CHENG C, et al. *Remaining useful life prediction of lithium-ion batteries with adaptive unscented kalman filter and optimized support vector regression* [J]. Neurocomputing, 2020, 376: 95-102.

[24] WANG F J, ZHAO Z B, REN J X, et al. *A transferable lithium-ion battery remaining useful life prediction method from cycle-consistency of degradation trend* [J]. Journal of Power Sources, 2022, 521.

[25] QIU J S, FAN Y C, WANG S L, et al. *Research on the remaining useful life prediction method of lithium-ion batteries based on aging feature extraction and multi-kernel relevance vector machine optimization model* [J]. International Journal of Energy Research, 2022, 46(10) : 13931-46.

[26] LYU Z Q, WANG G, GAO R J. *Li-ion battery prognostic and health management through an indirect hybrid model* [J]. Journal of Energy Storage, 2021, 42.

[27] FENG H L, SONG D D. *A health indicator extraction based on surface temperature for lithium-ion batteries remaining useful life prediction* [J]. Journal of Energy Storage, 2021, 34.

[28] DENG Z W, HU X S, LIN X K, et al. *General Discharge Voltage Information Enabled Health Evaluation for Lithium-Ion Batteries* [J]. Ieee-Asme Transactions on Mechatronics, 2021, 26(3) : 1295-306.

[29] GUPTA S, DEEP K. *Enhanced leadership-inspired grey wolf optimizer for global optimization problems* [J]. Engineering with Computers, 2020, 36(4) : 1777-800.

[30] LIU H Q, HUA G, YIN H S, et al. *An Intelligent Grey Wolf Optimizer Algorithm for Distributed Compressed Sensing* [J]. Computational Intelligence and Neuroscience, 2018, 2018.

[31] YANG X S, DEB S. *Cuckoo search: recent advances and applications* [J]. Neural Computing & Applications, 2014, 24(1) : 169-74.

[32] LONG W, JIAO J J, LIANG X M, et al. *An exploration-enhanced grey wolf optimizer to solve high-dimensional*

numerical optimization [J]. Engineering Applications of Artificial Intelligence, 2018, 68: 63-80.

[33] KOHLI M, ARORA S. *Chaotic grey wolf optimization algorithm for constrained optimization problems* [J]. Journal of Computational Design and Engineering, 2018, 5(4) : 458-72.

[34] XIE Y X, WANG S L, FERNANDEZ C, et al. *Improved gray wolf particle filtering and high-fidelity second-order autoregressive equivalent modeling for intelligent state of charge prediction of lithium-ion batteries* [J]. International Journal of Energy Research, 2021, 45(13) : 19203-14.

[35] LIU J Y, WEI X X, HUANG H J. *An Improved Grey Wolf Optimization Algorithm and its Application in Path Planning* [J]. Ieee Access, 2021, 9: 121944-56.

[36] ZHANG Z C, HONG W C, LI J C. *Electric Load Forecasting by Hybrid Self-Recurrent Support Vector Regression Model With Variational Mode Decomposition and Improved Cuckoo Search Algorithm* [J]. Ieee Access, 2020, 8: 14642-58.